



HAL
open science

Experimental and theoretical study of heat and mass transfer in a continuous, vertical and coaxial pyrolysis reactor for high porosity biochar production

Valentin Chataigner, Dominique Tarlet, François Ricoul, Jérôme Bellettre

► To cite this version:

Valentin Chataigner, Dominique Tarlet, François Ricoul, Jérôme Bellettre. Experimental and theoretical study of heat and mass transfer in a continuous, vertical and coaxial pyrolysis reactor for high porosity biochar production. *Fuel*, 2023, 351, pp.128848. 10.1016/j.fuel.2023.128848 . hal-04140911

HAL Id: hal-04140911

<https://hal.science/hal-04140911>

Submitted on 26 Jun 2023

HAL is a multi-disciplinary open access archive for the deposit and dissemination of scientific research documents, whether they are published or not. The documents may come from teaching and research institutions in France or abroad, or from public or private research centers.

L'archive ouverte pluridisciplinaire **HAL**, est destinée au dépôt et à la diffusion de documents scientifiques de niveau recherche, publiés ou non, émanant des établissements d'enseignement et de recherche français ou étrangers, des laboratoires publics ou privés.

Experimental and theoretical study of heat and mass transfer in a continuous, vertical and coaxial pyrolysis reactor for high porosity biochar production

Valentin CHATAIGNER^{a,b}, Dominique Tarlet^b, François Ricoul^c, Jérôme Bellettre^b

^aFlorentaise, Le Grand Pâtis, 44850 Saint Mars du Désert, France

^bNantes Université, Laboratoire de Thermique et Energie de Nantes LTeN UMR CNRS 6607, France

^cS3d Ingénierie, Groupe Keran 4 Rue René Viviani, 44200 Nantes, France

Highlights

- Tests on a patented continuous, vertical and coaxial pyrolysis reactor
- Reaching the thermokinetic conditions for pyrolysis in order to obtain a biochar with a specific surface of 200m²/g from pine bark
- Acquiring the parameters of the Arrhenius formalism adapted to pine bark
- Development of a numerical model and comparison of theoretical and experimental results

Abstract

The development of a high porosity biochar production facility to meet an industrial need requires a detailed knowledge of the thermochemical phenomena of pyrolysis. The main challenge of this work is the production of biochar with a high porosity in large quantities, and producing a residual gas that can be used for drying biomass. Two complementary tools have

been here developed and operated: a patented prototype and a designing numerical model. The model was developed in parallel with tests on the prototype and a characterisation phase of the various materials involved in the pyrolysis process in order to increase the correspondence between numerical model and experimental results. The model is used to predict, depending on the geometry chosen, the temperature in the pyrolysis zone, the heating rate and residence time corresponding to the applied biomass flow rate, as well as the biochar and gas mass yields.

This study demonstrated the ability of the experimental plant to produce a high porosity biochar with a specific surface of $200 \text{ m}^2 \cdot \text{g}^{-1}$ in the best case and a constant carbon content around 90% on dry basis due to the separation of the partial oxidation and pyrolysis zones. Following a material characterisation phase and a customisation of the parameters of the Arrhenius formalism adapted to pine bark, the numerical model shows a strong correspondence in terms of temperatures, biochar yield and thermochemical kinetics with the experimental observations from the prototype.

Keywords: pine bark pyrolysis, vertical pyrolyser, pyrolysis modelling, high porosity biochar.

Nomenclature

Latin letters		
A	pré-exponential factor	(s^{-1})
Cp	specific heat	$(\text{J} \cdot \text{kg}^{-1} \cdot \text{K}^{-1})$
d	diameter	(m)
E	activation energy	$(\text{J} \cdot \text{kg}^{-1})$

h	reactor height	(m)
H	species enthalpy	$(J.kg^{-1})$
L_v	latent heat	$(J.kg^{-1})$
\dot{m}	mass flow rate	$(kg.s^{-1})$
Q_{reaction}	reaction heat flux	(W)
r	radius	(m)
r_2	inner wall radius	(m)
r_3	outer wall radius	(m)
R	kinetic rate constant	(s^{-1})
t	time	(s)
T	température	$(^{\circ}C)$
T_1^0	reference temperature at 20°C	$(^{\circ}C)$
T_2^0	reference temperature at 100°C	$(^{\circ}C)$
u	velocity	$(m.s^{-1})$
z	vertical abscissa	(m)
Greek letters		
ε	bed porosity	$(-)$
ΔH	enthalpy of pyrolysis reaction	$(J.kg^{-1})$
λ^{eff}	effective thermal conductivity	$(W.m^{-1}.K^{-1})$
λ^{cond}	equivalent thermal conductivity by conduction	$(W.m^{-1}.K^{-1})$
λ^{rad}	equivalent thermal conductivity by radiation	$(W.m^{-1}.K^{-1})$

ρ	density	$(kg.m^{-3})$
ρ_{app}	biomass appparent density	$(kg.m^{-3})$
σ	Stephan-Boltzmann constant	
Subscripts		
c	char	
i	radial numerical indice	
j	vertical numerical indice	
k	solid or gas species	
g	uncondensable gas	
m	moisture	
s	steam	
t	tar	
w	wood	

1 Introduction

Biomass is an available ressource on earth for producing renewable energy. This energy source can be described as renewable since its carbon balance can be considered neutral. Indeed, biomass during its growth, absorbs CO_2 . Biomass as such is not considered as energy. It has to be converted from a raw, carbon-rich material into usable energy in the form of heat, electricity or mechanical energy. There are several processes that allow this conversion. The well-known technology for converting biomass into energy by thermochemical means is combustion. Combustion is the oldest method of converting biomass. The combustion is at

the origin of the development of humans, firstly through the use of biomass and more recently, following the industrial revolution, through the use of fossil fuels. These fossil fuels are abundant, cheap and easily transportable and usable. However, fossil fuel combustion is both the source of many advances in the use and consumption of energy, but also one of the main sources of greenhouse gas emissions, in particular CO_2 . This is why pyrolysis has been gaining interest in recent years as a solution for "carbon sequestration". Unlike combustion, pyrolysis has low carbon consumption and CO_2 emissions. To offset greenhouse gas emissions caused by human activity, Werner et al. [1] indicate that between 100 and 300 Gt of biochar by pyrolysis would need to be produced to achieve carbon neutrality and keep global warming below $1.5^\circ C$.

The development of human activity has not only an impact on air quality, but also on soil quality. Indeed, given the strong growth of the world's population, agricultural and industrial production has turned to chemicals to increase their production capacity. Unfortunately, these production methods are now reaching their limits because they degrade crop supports. In this sense, pyrolysis can provide an answer to this problem. Pyrolysis produces indeed a solid residue called biocarbon, biochar or coke. Biochar is a carbon-rich solid derived from a biomass or globally from a biobased material. Depending on the pyrolysis conditions and the nature of the biomass used, this biochar has a more or less developed porous structure. Depending on the size of its pores, the biochar can adsorb different compounds such as water, nutrients or pollutants, mostly in soils or aqueous media. This biochar has the advantage of being easily integrated into the soil for carbon sequestration due to its solid form and its stability for decades or even centuries. In this context, biochar has a key role to play in the adsorption of chemical substances and on soil improvement. This agronomic aspect of the

project raises new questions about the adjustment of pyrolysis parameters and directs the way of controlling the understanding of the thermochemical mechanisms of biochar formation in order to bring it to favourable characteristics for its agronomic valorisation. The originality of this project is therefore to couple the thermal and energetic performances of a pyrolysis system with an optimisation of the properties of the biochar products from pyrolysis. The production of biochar is subject to a double compromise between biochar properties and thermokinetic parameters of pyrolysis, but also between quality and quantity produced.

This research is based on numerous references that have been used to understand the thermochemical kinetics of pyrolysis, to guide the strategic choice of piloting and to help to build a pyrolysis model. Indeed, Shafizadeh et Chin [2] established a work that was used as a basis for a multitude of later studies on the thermochemical degradation of wood as for examples, the works of Graham et al. [3] about the cellulose fast pyrolysis or that of Hameed et al. [4] on cellulose pyrolysis in fluidized bed reactor. Richter et Rein [5] studied pyrolysis at microscopic scale by analysing the strength of wood as a function of the time the material was exposed to heat at a defined temperature. Based on this work, Thurner and Mann [6] studied pyrolysis in a four-species reaction scheme in three parallel reactions with wood as reactant and biochar, gas and tar as products. The reaction energies are introduced into the modelling of conversions by pyrolysis. Di Blasi [7] also characterised the mechanisms of thermochemical degradation of wood by comparing a global reaction model and another multi-reaction scheme over a temperature range of 300 to 400°C. Bryden et al. [8] developed a global wood pyrolysis model with simulations on different particle sizes and humidities as a sensitivity study to quantify the influence of intrinsic pyrolysis parameters. In addition, Lamarche et al.

[9] have modelled the pyrolysis of wood pellets in an unsteady regime in an externally heated reactor.

Almost all the work carried out uses laboratory-scale measurement tools to observe the thermochemical conversion of biomass. Thurner and Mann [6] report for example the kinetic pyrolysis parameters obtained in an isothermal tube furnace with oak, Wagenaar et al. [12] in a drop tube for pine and Di Blasi and Branca [13] for beech in a tube furnace. In this study, the thermochemical conversion of biomass will be observed under semi-industrial conditions.

The present work studies and model the heat and mass flows in a vertical and coaxial patented pyrolyser with an annular pyrolysis zone and an internal heated zone. The aim of the project is to produce a biochar that meets quality specifications by converting pine bark, which is almost not studied in the various pyrolysis studies. Pinto et al. [10] used only pine bark tanins for producing catechols and Jahiding et al. [11] used pine bark but for bio-fuel producing.

This work complements numerical and experimental studies of Tobo et al. [14] and Lamarche et al. [9] on externally heated pyrolysers with a tubular geometry. The study edited by Zhong et al. [15] also provides an understanding of biomass mass loss mechanisms with the construction of a biomass conversion prediction algorithm and a comparison of theoretical and experimental results.

The pyrolysis parameters will be studied by carrying out tests on a prototype. This prototype was first used in a gasifier configuration to study the coupling with a SOFC stack in the work of Ricoul et al. [16]. In order to meet coal production needs, this prototype was then changed into a pyrolyser configuration. It consists of three coaxial zones with partial oxidation in the central part, pyrolysis in the intermediate annular zone and recirculation of the hot gases in

the outer annular space. This design, in which the partial gas oxidation and pyrolysis zones are separate, allows the evacuation of residual gas from the partial oxidation, which facilitates thermal regulation and control by evacuating the excess energy. This waste gas, has low CO_2 emissions when burnt in a flare at the end of the process.

A high quality biochar must have a specific surface area above $300\text{ m}^2.\text{g}^{-1}$ and a carbon content close to 90% on dry matter. These agronomic targeted characteristics of biochar have been tested and validated in field trials. The numerical model developed, allows the characterisation of the material conversion chains and the thermal kinetics during pyrolysis. This numerical model is the subject of a thermochemical coupling between heat diffusion in the pyrolysis bed and the consumption and production of materials. The approach of the paper is to carry out the development of a numerical dimensioning tool and physical experimentation on the pyrogasification prototype in parallel to then compare the results and validate the model.

The experimental and numerical tools will first be presented. Then the results of the tests on the pyrolysis prototype will be presented. The experimental analysis will be compared with the theoretical results of the numerical model with the mass-energy balances, temperatures in the pyrolysis zone and thermokinetic parameters. In conclusion, the main research indicators of this paper will be recalled before an opening on the continuation of this study.

2 Materials and methods

2.1 Pyrolysis pilot unit

2.1.1 Installation and instrumentation description

The patented pyrolysis prototype named "Ariane" has the particularity of being vertical and

coaxial. Its design, shown in Fig. 1, is based on the interlocking of three cylinders forming three distinct zones and allowing the separation of the partial oxidation and pyrolysis zones.

Partial oxidation of the

pyrolysis gases in the

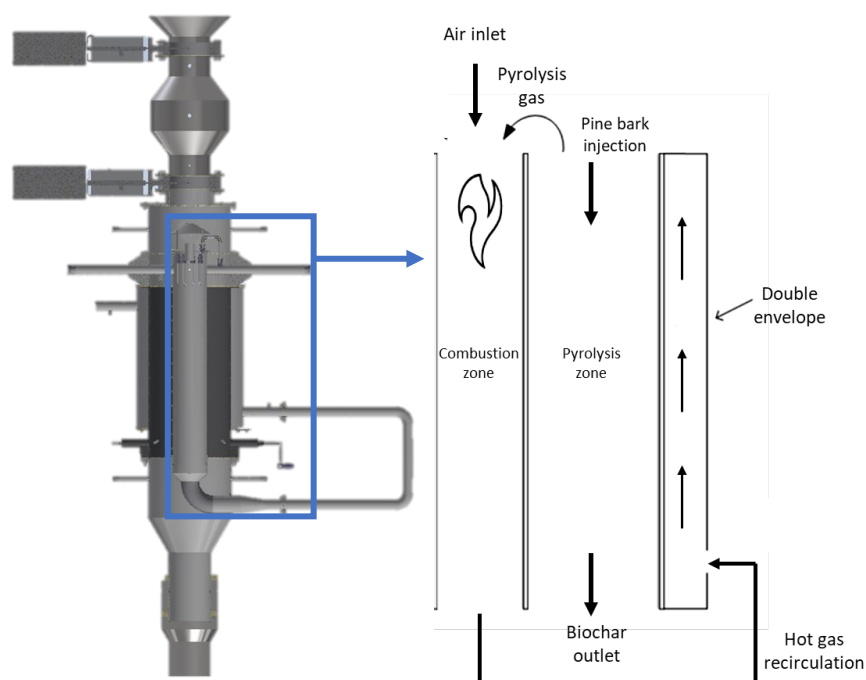


Fig. 1. Pyrolysis unit conception and flows circulation (axysimetric view)

combustion zone allows the system to be autothermal following a propane start-up phase that allows the thermochemical reactions of pyrolysis to be launched. This prototype consists of a pyrolyser, ancillary components, instrumentation and a gas post-treatment module. Contrary to the work of Daouk [17], the oxidation zone is separated from the pyrolysis zone which allows to control each reaction independently

The core of the study lies in the pyrolysis zone. This vertical annular space with a height of 0.8 m allows the thermochemical conversion of biomass after drying phase. The solid flows downwards and the gas flows upwards. This zone is heated by heat from the central cylinder

in which the pyrolysis gases are partially burned. At the periphery of this zone, a double envelope limits radial heat losses. The annular pyrolysis zone has an inner radius of 0.084 m and an outer radius of 0.2 m, giving a cross-sectional area of approximately 0.1 m². The flow circulation in axisymmetric view is shown in Fig. 1.

The pyrolysis zone is instrumented with three lines of N and K type thermocouples. A first thermocouple line close to the burner wall and a second close to the wall of the gas recirculation jacket. The thermocouples of the third line are integrated in a rod immersed in the pyrolysis bed in order to limit the effects of radiation from the hot and cold walls of the furnace and the jacket. 12 thermocouples spaced 7 cm the one each over are placed on each line.

The temperatures in the pyrolysis zone are controlled by the air factor in the furnace. Depending on the desired temperature level and the biomass flow rate of the test, the amount of energy released from the furnace to the pyrolysis zone varies. By adjusting the air flow in the furnace, close pyrolysis temperatures can be achieved regardless of the bark flow.

2.1.2 Biomass characterisation and preparation

Pine bark is the only biomass used in the study and comes from the company's resources in connection with its activity as a producer of potting soils and agricultural amendments. The bark has an initial

Table 1. Biomass characteristics

Quantity	Value
LHV on anhydrous [<i>MJ.kg</i> ⁻¹]	20,79
Lignin content [%]	44,3
Density [<i>kg.m</i> ⁻³]	208,4
Humidity [%]	13,59

particle size of 0 to 15 mm. In the first tests, the finest fraction of these barks disturbed the stability of the reactor flame. These barks were screened and now have a biomass particle size of 4 to 15 mm. The physico-chemical analysis of the barks is shown in Table 1.

As the trials were conducted over a long period of time, the storage conditions of the bark did not allow it to be totally sealed against external climatic conditions. The humidity of the bark varied from 12.5 to 16% depending on the season and climatic conditions.

2.1.3 Testing approach

The first objective of the tests is to obtain the maximum potential in terms of bark mass flow of the prototype. This maximum mass flow rate is largely dependent on the quality of the heat diffusion in the pyrolysis zone and thus indirectly on the geometry of the reactor. The main qualitative objective is to produce a biochar with the highest possible specific surface area with a target of $300 \text{ m}^2 \cdot \text{g}^{-1}$.

The flow rate of pine bark and the air flow rate injected into the furnace are the two parameters used to control a test. All other flows (coal, syngas, condensate) are dependent on these bark and air flow. The bark flow rate during the tests is gradually increased from $14 \text{ kg} \cdot \text{h}^{-1}$ until a flow of bark is reached that no longer ensures the thermochemical stability of the system. If the air flow rate and bark flow rate are too low, the thermal stability of the pyrolysis is not ensured.

Each flow was tested at least twice under different outdoor conditions. These external conditions in the current design of the pyrolyzer are experienced and cannot be changed (ambient temperatures, air, humidity...). These tests allow us to observe the thermochemical response of the pyrolyser under the most favourable and unfavourable test conditions. The results presented in section Results and discussion are based on an average of all the tests performed for each bark flow.

For each test over a range of bark flow rates from 14 to 30 $kg \cdot h^{-1}$, the injected air flow rate must allow thermochemical equilibrium to be achieved over a period of at least four hours. Four hours corresponds to the period during which the mass, thermal and chemical balances are established. Over this range of bark flow rates, the ratio between the air volume flow rate and the bark mass flow rate is 0.6 Nm^3 of air per kg of anhydrous bark. This ratio is stable over all the tests.

During each test, a sample of biochar representative of the test is taken for analysis of the specific surface area and its fixed carbon content, in order to define the flow of bark to obtain the best coal quality. For gas quality, an infrared technology analyser is placed on the syngas extraction line to the flare. This analyser measures CO , CO_2 , H_2 , CH_4 and O_2 levels to measure the residual dioxygen level or to detect possible air infiltration. As the

elemental compositions on dry basis of the bark and biochar are known and shown in Table 2, the mass and volume flow of each element of the pyrolysis gas can be obtained.

Table 2. Pine barks and biomass elemental composition

Contents	Pine barks	Biochar
Carbon [%db]	55.2	90.17
Hydrogène [%db]	5.5	1.6
Nitrogen [%db]	0.2	0.83
Oxygen [%db]	39.05	1.02

2.2 Pyrolysis thermochemical modelling

The development of the numerical model is an adaptation of the model developed by Lamarche et al. [9], to the particular geometry of the Ariane prototype. The Lamarche et al. [9] model required modifications to the intrinsic parameters of the pyrolysis co-products, the boundary conditions and the geometry, moving from a reactor whose pyrolysis zone is heated

only from the outside to a pyrolyser whose pyrolysis zone is heated from the inside and the outside according to the temperatures imposed on the walls of the updraft pyrolyser.

2.2.1 Model and hypothesis

The assumptions and considerations made for the modelling that correspond to a pseudo homogenous model are as follows:

- (a) Local thermal equilibrium between gas and solid phases $T_{gas} = T_{solid}$
- (b) 6 considered species : wood, coke, gas, tar, moisture and steam
- (c) Particle homogeneous in temperature and composition
- (d) Consideration of bed settlement by determining a variable bed speed
- (e) Particle size homogeneity
- (f) The contact between the bed and the heating walls is considered perfect (no contact resistance)
- (g) Variable mass heat capacities for water and steam and constant for wood, coke, gas and tar (controled by chemical analysis)

The pyrolysis zone is the site of two main thermochemical phenomena including biomass drying and biomass conversion by pyrolysis gas volatilization under heat flux.

The heat required to convert the biomass into pyrolysis co-products comes from the combustion zone in the centre of the pyrolysis zone where the pyrolysis gases from the bark are partially burnt.

2.2.2 Mass conservation

For translating mass conservation, Lamarche et al. [9] use the Arrhenius chemical kinetics formalism. The displacement of the bed introduces an additional term related to the

movement of the wood and then the coal downwards according to vertical abscissa. The consumed species are materialized by the negative sign and those produced by the positive sign. Considering the convection of the solid phase only along the vertical abscissa z :

Wood

$$\frac{\partial \rho_w}{\partial t} + \frac{\partial}{\partial z}(\rho_w u_s) = -\rho_w \cdot R_w \quad (1)$$

With R_w , reaction rate in $[s^{-1}]$ for wood consumption

Coke

$$\frac{\partial \rho_c}{\partial t} + \frac{\partial}{\partial z}(\rho_c u_s) = \rho_c \cdot R_c \quad (2)$$

With R_c , reaction rate in $[s^{-1}]$ for coke production

Moisture

$$\frac{\partial \rho_m}{\partial t} + \frac{\partial}{\partial z}(\rho_m u_s) = -\rho_m \cdot R_m \quad (3)$$

With R_m , reaction rate in $[s^{-1}]$ for moisture consumption

The biomass flows through the pyrogasification reactor from top to bottom. Any velocity going against this flow is defined negatively and vice versa. For the steam phase, it can be written :

Steam

$$\frac{\partial}{\partial z}(\rho_s u_s) = \rho_w \cdot R_s \quad (4)$$

With R_s , reaction rate in $[s^{-1}]$ for steam production during drying

Gas

$$\frac{\partial}{\partial z}(\rho_g u_g) = \rho_w \cdot R_g \quad (5)$$

With R_g , reaction rate in $[s^{-1}]$ for gas production

Tar

$$\frac{\partial}{\partial z}(\rho_t u_t) = \rho_w \cdot R_t \quad (6)$$

With R_t , reaction rate in [s^{-1}] for tar production

2.2.3 Energy conservation

The energy variation of a mesh takes into account its quantity of energy, the exchanges of materials with the meshes above and below (piston flow), the heat exchanges with the neighboring meshes and in another equation part the energy of drying and pyrolysis. The general energy equation for any species k is defined as follows:

$$\underbrace{\sum_k \frac{\partial}{\partial t}(\rho_k H_k)}_{\text{accumulation}} + \underbrace{\sum_k \text{div}(\rho_k H_k \vec{u}_k)}_{\text{convection}} - \underbrace{\text{div}(\lambda^{eff} \cdot \overrightarrow{\text{grad}}(T))}_{\text{thermal diffusivity}} = \underbrace{r_w \Delta H^0}_{\text{pyrolysis reaction}} + \underbrace{r_m L_v}_{\text{drying reaction}} \quad (7)$$

Separation of variables applied to the accumulation term

$$\sum_k \frac{\partial}{\partial t}(\rho_k H_k) = \sum_k \rho_k \frac{\partial H_k}{\partial t} + \sum_k H_k \frac{\partial \rho_k}{\partial t} \quad (8)$$

Divergence theorem applied to the convection term

$$\sum_k \text{div}(\rho_k H_k \vec{u}_k) = \sum_k H_k \cdot \text{div}(\rho_k \vec{u}_k) + \sum_k \rho_k \vec{u}_k \cdot \overrightarrow{\text{grad}}(H_k) \quad (9)$$

By injecting into the general equation,

$$\sum_k \rho_k \frac{\partial H_k}{\partial t} + \sum_k H_k \frac{\partial \rho_k}{\partial t} + \sum_k H_k \cdot \text{div}(\rho_k \vec{u}_k) + \sum_k \rho_k \vec{u}_k \cdot \overrightarrow{\text{grad}}(H_k) - \text{div}(\lambda^{eff} \cdot \overrightarrow{\text{grad}}(T)) = r_w \Delta H^0 + r_m L_v \quad (10)$$

The factorisation by H gives the mass balance equation which is reinjected in a second step,

$$\sum_k \rho_k \frac{\partial H_k}{\partial t} + \sum_k H_k \left(\frac{\partial \rho_k}{\partial t} + \text{div}(\rho_k \vec{u}_k) \right) + \sum_k \rho_k \vec{u}_k \cdot \overrightarrow{\text{grad}}(H_k) - \text{div}(\lambda^{eff} \cdot \overrightarrow{\text{grad}}(T)) = r_w \Delta H^0 + r_m L_v \quad (11)$$

$$\sum_k \rho_k \frac{\partial H_k}{\partial t} + \sum_k H_k r_k + \sum_k \rho_k \vec{u}_k \cdot \overrightarrow{\text{grad}}(H_k) - \text{div} \left(\lambda^{eff} \cdot \overrightarrow{\text{grad}}(T) \right) = r_w \Delta H^0 + r_m L_v \quad (12)$$

By posing,

$$c_{Pk} = \frac{\partial H}{\partial T} \quad (13)$$

Thus,

$$H_k = \int_{T_k^0}^T c_{Pk} dT \quad (14)$$

The final equation in 2D cylindrical coordinates taking into account the 1D convection term along z,

$$\begin{aligned} \sum_k \rho_k c_{Pk} \frac{\partial T}{\partial t} + \sum_k c_{Pk} r_k (T - T_1^0) \frac{\partial T}{\partial z} + \sum_k \rho_k u_k c_{Pk} \frac{\partial T}{\partial z} - \lambda^{eff} \left(\frac{\partial^2 T}{\partial z^2} + \frac{1}{r} \frac{\partial}{\partial r} r \frac{\partial T}{\partial r} \right) \\ = r_w \Delta H^0 + r_m L_v \end{aligned} \quad (15)$$

By explaining the set of species defined by the k species, $Q_{reaction}$, representing the power density dissipated during the reaction can be explained,

$$\begin{aligned} (\rho_w c_{Pw} + \rho_c c_{Pc} + \rho_m c_{Pm}) \frac{\partial T}{\partial t} + [(u_s (\rho_w c_{Pw} + \rho_c c_{Pc} + \rho_m c_{Pm})) \\ (\rho_g u_g c_{Pg} + \rho_t u_g c_{Pt} + \rho_s u_s c_{Ps})] \frac{\partial T}{\partial z} - \lambda^{eff} \left(\frac{\partial^2 T}{\partial z^2} + \frac{1}{r} \frac{\partial}{\partial r} r \frac{\partial T}{\partial r} \right) = Q_{reaction} \end{aligned} \quad (16)$$

$$\begin{aligned} Q_{reaction} = \rho_m R_m ((T - T_2^0)(c_{Pm} - c_{Ps}) - L_v) + \\ \rho_w ((T - T_1^0)(c_{Pw} R_w - c_{Pc} R_c - c_{Pg} R_g - c_{Pt} R_t) - R_w \Delta H^0) \quad [kW.m^{-3}] \end{aligned} \quad (17)$$

With $T_1^0 = 20^\circ C$, enthalpy reference temperature of pyrolysis reactions

$T_2^0 = 100^\circ C$, vaporisation temperature of water at atmospheric pressure

2.2.4 Boundary conditions

The boundary conditions depend on the direction of flow of the gas phase. In this case, the gas phase flows from the bottom to the top, against the direction of the biomass. The reactor shell is an impermeable wall with no species transfer.

2.2.4.1 Mass

The mass boundary conditions do not differ between species. It can thus be written for pyrolysis zone in accordance with the reactor scheme (Fig. 1).

Reactor top ($z=0$) : the wet biomass is introduced at the top of the reactor

$$\rho_w(r, 0) = \rho_{app}(1 - HR) \quad \forall r_2 < r < r_3 \quad (18)$$

$$\rho_m(r, 0) = \rho_{app}HR \quad \forall r_2 < r < r_3 \quad (19)$$

$$\rho_c(r, 0) = 0 \quad \forall r_2 < r < r_3 \quad (20)$$

Gases are exhausted on the top of the reactor,

$$\frac{\partial(\rho_j u_j)}{\partial z}(z = 0) = 0 \quad \forall j = g, t, s \quad \forall r_2 < r < r_3 \quad (21)$$

Reactor bottom ($z=h$) : The biochar (and non-pyrolysed wood, if any) is removed from the bottom of the reactor,

$$\frac{\partial(\rho_i u_i)}{\partial z}(z = h) = 0 \quad \forall i = w, c, m \quad \forall r_2 < r < r_3 \quad (22)$$

$$\rho_j(r, h) = 0 \quad \forall j = g, t, s \quad \forall r_2 < r < r_3 \quad (23)$$

Combustion wall ($r=r_2$) :

$$\frac{\partial \rho_k}{\partial r}(r = r_2) = 0 \quad \forall k = g, t, s, w, c, m \quad \forall 0 < z < h \quad (24)$$

Hot gas wall ($r=r_3$) :

$$\frac{\partial \rho_k}{\partial r}(r = r_3) = 0 \quad \forall k = g, t, s, w, c, m \quad \forall 0 < z < h \quad (25)$$

2.2.4.2 Heat transfer

The thermal boundary conditions are specific to the reactor under consideration and are dependent in this case on the temperatures of the furnace and jacket walls.

2.2.4.2.1 Vertical boundary conditions

A variable temperature as a function of height is thus imposed according to the results obtained following tests on the internal (core) and external (hot gas recirculation jacket) vertical walls. As the thermocouples for defining the vertical thermal boundary conditions are on the side of the pyrolysis bed in the bark and biochar, no contact resistance between the vertical hot walls and the pyrolysis bed is considered. Thus, T_{12} will represent the temperature of the firewall, and T_{23} will represent the temperature of the hot gas wall. Both temperatures depend on the vertical position considered, such as:

$$T_{12} = T(r_1, z) = T(r_2, z) \quad \forall 0 < z < h \quad (26)$$

$$T_{23} = T(r_2, z) = T(r_3, z) \quad \forall 0 < z < h \quad (27)$$

These temperatures are measured and averaged on time during the tests with different biomass flows from 14 to 30 $kg \cdot h^{-1}$, on the outside walls and are implemented in the model according to trend curves presented in Fig. 2.

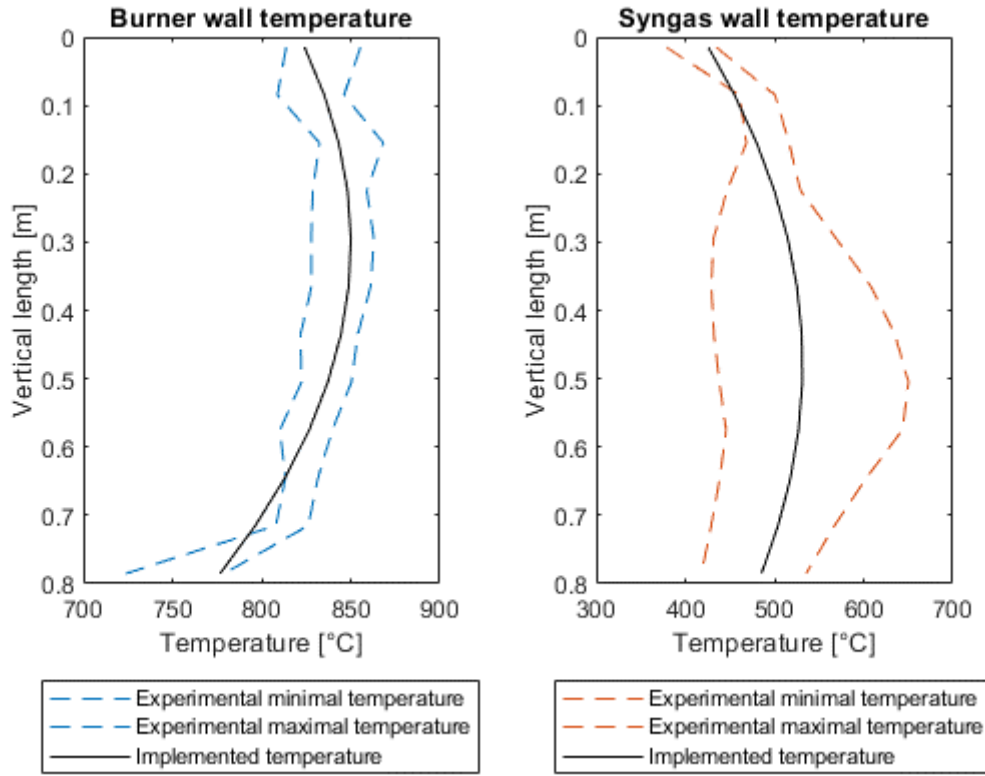


Fig. 2. a) Burner wall temperature and b) syngas wall temperature average, measured during the tests

2.2.4.2.2 Top boundary condition

The boundary conditions on the biomass inlet and biochar outlet zones are more complex to characterise. It will be considered that the upper boundary of the device will be topped by biomass waiting to be introduced into the reactor. Thus it can be considered that,

$$T(r, h) = T_{in} \quad \forall r_2 < r < r_3 \quad (28)$$

With T_{in} , initial temperature of the biomass which will be assessed at 20°C

2.2.4.2.3 Bottom boundary condition

For the lower wall it will be assumed that no conductive exchange will be active after this boundary. Thus, only the energy induced by the particles leaving the bed will be taken into account,

$$\vec{n} \cdot (\lambda^{eff} \nabla T) = 0 \quad \forall r_2 < r < r_3 \quad (29)$$

2.2.5 Initial condition

Any unsteady system requires initial conditions to be set before the simulation. They only have an influence on the calculation time. Indeed, when the initial conditions are close to the final solution, the calculation time is reduced. As for the boundary conditions, there are mass and thermal initial conditions.

2.2.5.1 Mass

The volume of the biomass bed is defined according to the reactor geometry,

$$v = \pi(r_3^2 - r_2^2) \cdot h \quad (30)$$

The initial mass input conditions take into account only the density and moisture content of the particle bed. It is thus possible to deduce the initial concentration of each species at t_0 .

- The initial dry wood concentration is defined as follows,

$$\rho_{w0} = \rho_{app} \left(1 - \frac{HR}{100} \right) \quad \forall (r, z) \in v \quad (31)$$

- The initial moisture concentration is given by,

$$\rho_{w0} = \rho_{app} \left(\frac{HR}{100} \right) \quad \forall (r, z) \in v \quad (32)$$

No other species are introduced into the reactor in the initial state, so,

$$\rho_{i0}(r, z, 0) = 0 \quad \forall i = c, g, t, s \quad \forall (r, z) \in v \quad (33)$$

2.2.5.2 Heat transfer

The initial thermal conditions are relative to the species present in the reactor at time $t = 0$ in the reactor. Thus the biomass bed is at room temperature, corresponding to the biomass inlet temperature.

$$T(r, z, 0) = T_{in} \quad \forall (r, z) \in \mathbb{V} \quad (34)$$

The initial temperature of the domain is set in fonction of pine bark flow between 100 or 150 °C to make the model converge more quickly and thus reduce the calculation time.

2.2.6 Effective thermal conductivity

The effective thermal conductivity is a quantity that allows the characterisation of heat transfer, particularly in porous media when these are subject to multiple heat transfer mechanisms. Thermal conductivity is used to characterise the dominant heat transfer in porous media: conduction and radiation. This concept takes into consideration both the solid and the cavities or pores of this solid. Bryden et al. [8] explain this concept by separating conductive and radiative terms.

$$\lambda^{eff} = \lambda^{cond} + \lambda^{ray} \quad (35)$$

With λ^{cond} , conduction contribution [$W \cdot m^{-1} \cdot K^{-1}$]

λ^{ray} , radiative contribution [$W \cdot m^{-1} \cdot K^{-1}$]

The author considers the terms λ^{cond} by weighting it by the mass proportion of moisture and wood and λ^{ray} such as,

$$\lambda^{cond} = \lambda_m + \eta_w \lambda_w + (1 - \eta_w) \lambda_c \quad [W \cdot m^{-1} \cdot K^{-1}] \quad (36)$$

$$\lambda^{rad} = \frac{\varepsilon}{1 - \varepsilon} \cdot \sigma \cdot \varphi_{pores} \cdot d_{pores} \cdot 4T^3 \quad [W \cdot m^{-1} \cdot K^{-1}] \quad (37)$$

The radiation term is insignificant compared to conduction for low temperatures but becomes the driving force for inter-particle heat exchange for high temperatures ($> 200^{\circ}\text{C}$). The pore diameter therefore has little or no influence at moderate temperatures.

The estimation of this particular conductivity is well known for moderate temperatures or for small temperature ranges, but is still in the research stage for high temperatures and for large temperature range. This conductivity is not well known for wood despite the work of Ragland et al. [18], TenWolde et al. [19] or Gupta et al. [20] but also for biochar although Perry et al. [21], Koufopoulos et al. [22] or Kantorovich and Bar-Ziv [23] have worked on the subject. They have worked at low or reduced temperature ranges or for charcoal on biochar that has been pyrolysed at different temperatures.

The adjustment of the parameters of the Arrhenius formalism and of the effective thermal conductivity were done in the present work in parallel. The objective was to tend towards an anhydrous biochar yield close to the experimental one and to make the pyrolysis temperatures coincide. This adjustment was made empirically using some of the experimental data. Then other experimental data are used to validate the model.

This difficulty in estimation at bed scale is due to the changing characteristics of the material during drying, pyrolysis and beyond pyrolysis. Finally, the effective thermal conductivity implemented which defines the thermal component of pyrolysis is:

$$\lambda^{eff}(T) = 2.21 \times 10^{-3}T - 0.25 \quad (38)$$

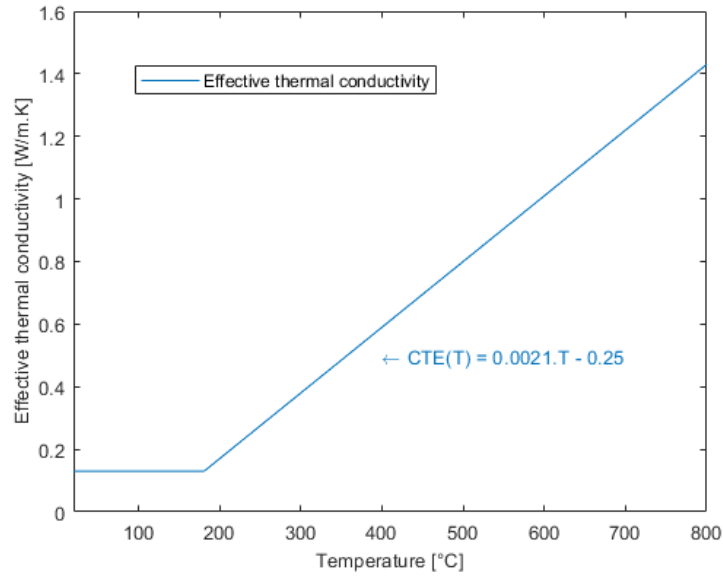


Fig. 3: Pyrolysis bed effective thermal conductivity

The majority of the authors quoted above mention a radiation which becomes the majority in the thermal exchanges in front of the conduction around 200°C. This is why for a temperature below 180°C the effective thermal conductivity has been taken at a constant value of 0.13 $W \cdot m^{-1} \cdot K^{-1}$.

Some authors like Gupta et al. [20] with 0.48 for bed scale bark take effective thermal conductivity values independent of temperature. The majority of the values found in the literature are only valid over a short temperature range. The most interesting representation of the dependence of the effective thermal conductivity for this study is the one presented by Kantorovich and Bar-Ziv [23] over a wide temperature range from 300 to 1100 K with an ETC increasing from 0.4 to 1.3 $W \cdot m^{-1} \cdot K^{-1}$.

2.2.7 Arrhenius formalism

Material conversion kinetics are defined by the Arrhenius formalism used by many authors such as Thurner and Mann [6], Lamarche et al. [9] and Stamm and Harris [24]. This formalism makes possible to translate a reaction rate R as a function of temperature by the expression :

$$R = A \exp\left(\frac{-E}{RT}\right) \quad [s^{-1}] \quad (39)$$

In this expression, the pre-exponential factor A , defines the intensity of the reaction while the activation energy E , defines at which temperature level the reaction takes place. A reaction rate must be defined for each species considered. The reaction scheme can be defined according to several scales. In the literature, the macroscopic scale is most often used, it considers biomass and its humidity at the process input and the usual pyrolysis co-products at the output such as biochar, pyrolysis gas or tars. The microscopic scale considers biomass as a mixture of cellulose, hemicellulose and lignin in different fractions depending on the biomass considered. Each of these components are converted into biochar, pyrolysis gas and tars as for the macroscopic scale.

Finally, the elementary scale is sometimes retained by considering the biomass according to its elementary fractions in C, H, N and O. It makes it possible to evaluate the fraction of these elements found in the co-products of pyrolysis. This reaction scheme makes it possible, among other things, to estimate the carbon content of the biochar.

In order to build a designing program, a global vision of the thermochemical reactions is suitable. Thus the macroscopic scheme is retained for this study. Our study considers six species, moisture, water vapour, wood, coke, tars, and incondensable gases. The chosen reaction scheme is indicated in Fig. 4:

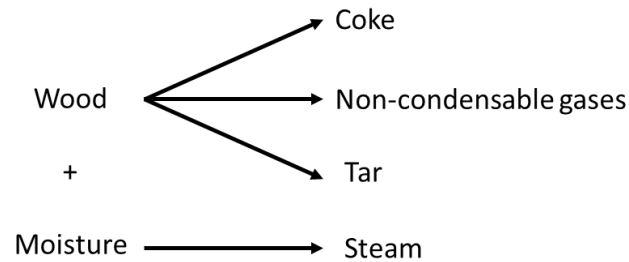


Fig. 4. Pyrolysis reaction scheme considered

In order to respect at all points and for all temperatures the mass balance between the different species of the model, Shafizadeh and Chin [2] defines the reaction rate of wood as the sum of pyrolysis co-products from wood:

$$R_w = R_c + R_g + R_t \quad [s^{-1}] \quad (40)$$

The pre-exponential factor as well as the activation energy are therefore given for each species as a function of the temperatures observed in the prototype. Only the parameters of the drying step are fully derived from the work of Bryden et al. [8]. As the pyrolysis reaction is endothermic, the reaction rates allow to translate the coupling between heat transfer and chemical conversion of the material. The parameters obtained are a variant of Thurner and Mann [6] parameters and are indicated in Table 3. It is indeed essential to adapt and personalise the Arrhenius parameters for each different case. The pre-exponential factor establishes the width of the temperature range over which the pyrolysis reaction takes place and the activation energy plays a role in the temperature at which the reaction takes place.

Following a sensitivity study on each parameter for each species, it turned out that only the pre-exponential factors need to be changed from the Arrhenius parameters of Thurner et Mann [6] for wood pellets.

Table 3. Arrhenius chemical parameters

	$A [s^{-1}]$	$E [J.mol^{-1}]$
Coke	9.92×10^4	1.065×10^5
Non condensable gases	2.18×10^3	8.86×10^4
Tar	4.54×10^5	1.127×10^5
Wood	$R_c + R_g + R_t$	
Steam – Moisture	5.13×10^{10}	8.8×10^4

The thermogravimetric analysis shown in Fig. 5 allows to obtain the correspondence between temperature and conversion of biomass into biochar. Despite the granulometry was different between thermogravimetric analysis and tests on the prototype with non modified biomass, this TGA was used for base to obtain the adapted pre-exponential factors. The TGA tests were reproduced four times, twice with nitrogen and twice with argon. Changing the inert gas had little effect on the results which showed minor differences between tests.

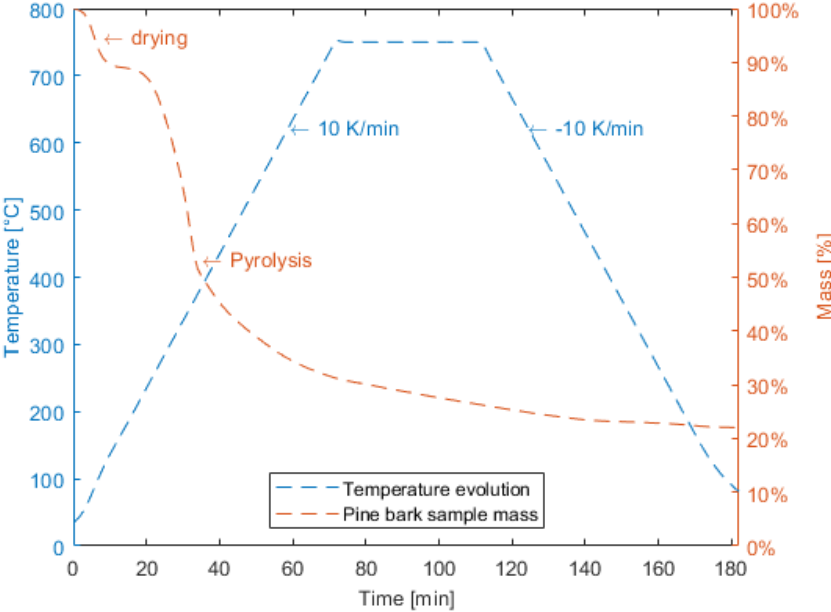


Fig. 5: Pine bark powder thermogravimetric analysis

Tinney [25] working on small wooden dowels, Agarwal [26] modelling the pyrolysis of a biomass composed of 100% cellulose and Roberts [27] with the pyrolysis of a wood composed of lignin, cellulose and hemicellulose show that the Arrhenius parameters depend on the granulometry, the type of biomass and its composition.

2.2.8 Problem-solving method

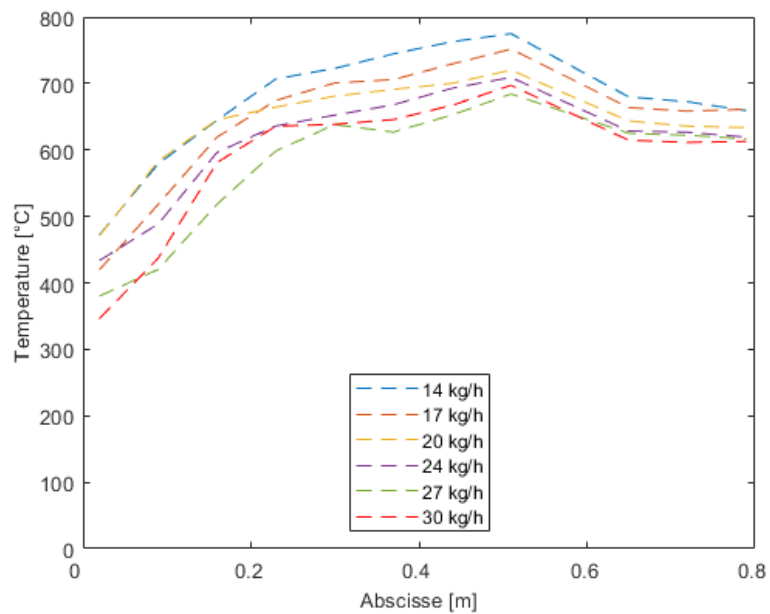
The thermochemical problem of pyrolysis was solved using an explicit method defined in transient regime. The chosen time step of 0.1 seconds allows an independance of the results even if the time step is modulated in the range [0.01 – 0.1s]. The same kind of tests were done for the mesh density. The vertical mesh is regular unlike the radial mesh which is radius dependent with a larger dr when the radius is small and a smaller dr when the radius is large. This radial variation of $dr(r)$ makes it possible to have equal horizontal exchange surfaces whatever the radius considered. The calculating time is under 5 *min* with a time step of 0.1 s, 22 radial divisions and 200 vertical divisions. The overall modelling scheme is presented in Annex A. This numerical model was developed in Matlab® for the universality of its language in the world of scientific research and its language close to C.

3 Results and discussion

3.1 Pyrolysis centre temperatures

As already explained, the temperature in the centre of the pyrolysis zone is measured via a stick in the center of the biomass bed consisting of 12 N-type thermocouples. Fig. 6 gives the

expression of temperatures as a function of the wet bark flow rate and the altitude in the pyrolysis zone. Point 0 is the top of the reactor and 0.8 m is the bottom.



The thermal diffusion Fig. 6. Experimental pyrolysis temperature evolution

from the flame, to the core to provide the energy for the endothermic pyrolysis reaction can be clearly seen between 0.2 and 0.5 m. As the flame is positioned in the upper part of the furnace, the thermal energy is diffused in the upper part of the reactor into the drying cylinder. For these reasons, the temperature at which the bark enters the pyrolysis zone is at least 350°C for a bark flow rate of $30\text{ kg}\cdot\text{h}^{-1}$. The pyrolysis of the bark therefore starts before it enters the pyrolysis zone. The maximum temperature reached by the bark is 780°C for the lowest flow rate, i.e. $14\text{ kg}\cdot\text{h}^{-1}$.

All the curves follow the same trend as a function of the vertical abscissa. The average pyrolysis temperature decreases with the bark flow rate. A difference of about one hundred

degrees is visible between the bark flow rates 14 and 30 $kg \cdot h^{-1}$. Although the flow rate has doubled, this difference remains moderate given the small width of the pyrolysis zone, which allows heat transfer to take place despite the variations in flow rate. The quantity of gas oxidised in the furnace also increases with the flow rate, which gives back to the bark a greater fraction of energy when the flow rate increases.

The theoretical and experimental curves in Fig. 7 show a sufficient correspondence for the validation of the numerical model. The theoretical curves start upstream of the pyrolysis zone (abscissa 0) since implementing an inlet temperature of a few hundred degrees (which corresponds to a pyrolysis temperature) does not allow for model convergence. The input temperatures of the bark and initial, for a convergence of the model, must be located before the drying or between the drying and the pyrolysis (lower than $80^{\circ}C$ or between 130 and $180^{\circ}C$).

No thermocouple on the prototype allows to validate the evolution of temperatures upstream of the pyrolysis zone in order to confirm the parameters of the numerical model on this zone.

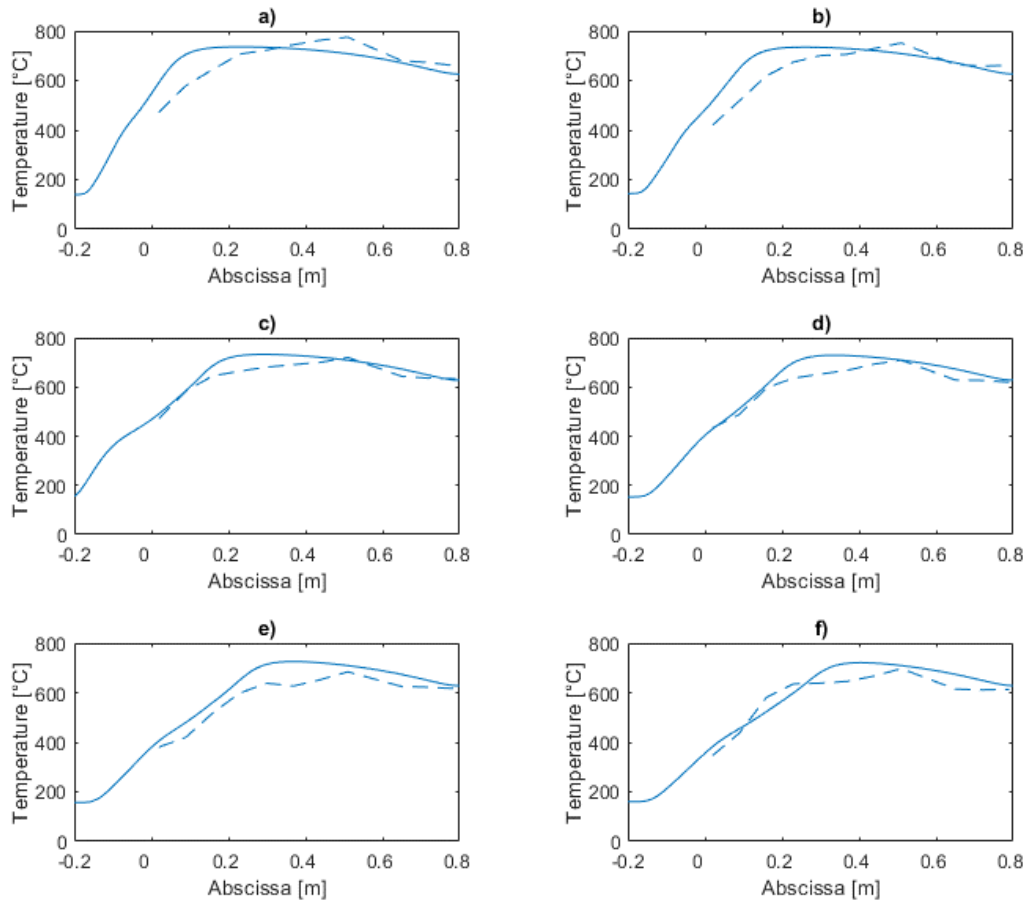


Fig. 7. Experimental -- and theoretical - temperatures comparison at 14 kg/h (a), 17 kg/h (b), 20 kg/h (c), 24 kg/h (d), 27 kg/h (e) and 30 kg/h (f) of wet biomass

3.2 Residence time and heating rate

The residence time of the biomass in the pyrolysis zone is obtained by matching an ATG analysis with the temperatures observed at the different levels of the pyrolysis zone. In fact, since the correspondence between mass loss and temperature is obtained by GTA, the velocity of the pyrolysis bed can be deduced as a function of temperature. The total residence time of a bark particle in the pyrolysis zone can then be obtained. Moreover, the densities of the incoming wet biomass and the outgoing coal are relatively close, which limits the correction of the residence time by the evolution of the density. When measuring the quality

of the biochar (specific surface, fixed carbon content...), the residence time corresponding to the best quality biochar can be deduced.

The temperature at which the bark enters the pyrolysis zone is at least 350°C, the heating rate is deduced from the temperature readings of the thermocouples upstream of the pyrolysis zone and from the first thermocouples in the pyrolysis zone. Knowing their vertical spacing, the heating rate can be deduced.

The heating rates and temperature levels observed correspond rather to rapid pyrolysis. The results are presented in Fig. 8. However, the mass fractions of the co-products are

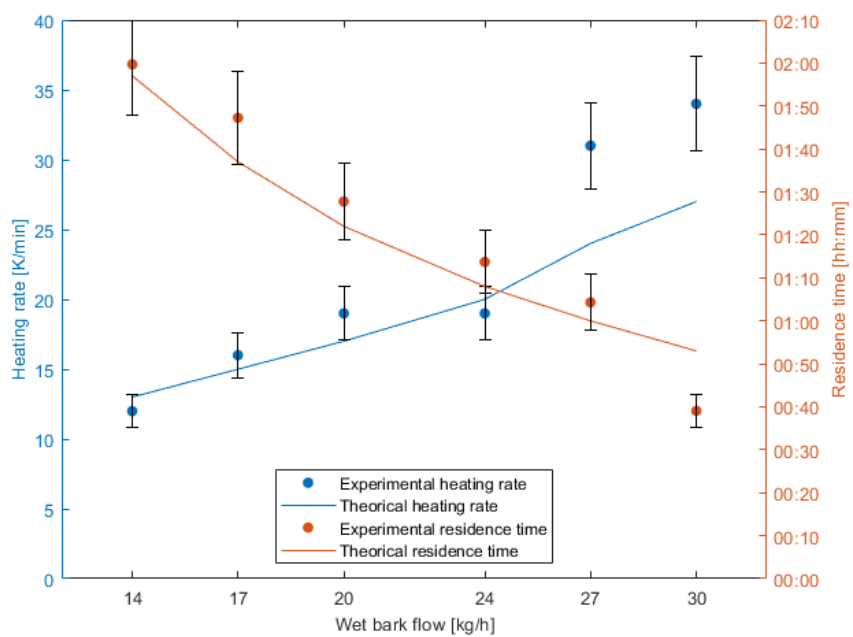


Fig. 8. Experimental and theoretical heating rates and residence time comparison with anhydrous coke yields ranging from 36 to 41% depending on the bark flow rates and therefore between 59 and 64% volatiles.

Ricoul et al. [16] define the limits of each type of pyrolysis in terms of temperature level, heating rate and co-product yields shown in Table 4.

Table 4 Features of each type of pyrolysis [16]

Pyrolysis type	Temperature level	Heating rate	Major products
Slow	400 – 600 °C	1 – 10 °C.min ⁻¹	Coke (30-40%) Volatiles (60-70%)
Fast	600 – 800 °C	10 – 50 °C.min ⁻¹	Coke (20-25%) Volatiles (75-80%)
Flash	600 – 900 °C	> 50 °C.min ⁻¹	Coke (10-20%) Volatiles (80-90%)

3.3 Mass yields

The distribution of the mass yields of biochar, condensate and syngas in Fig. 9 changes little as a function of wet bark throughput.

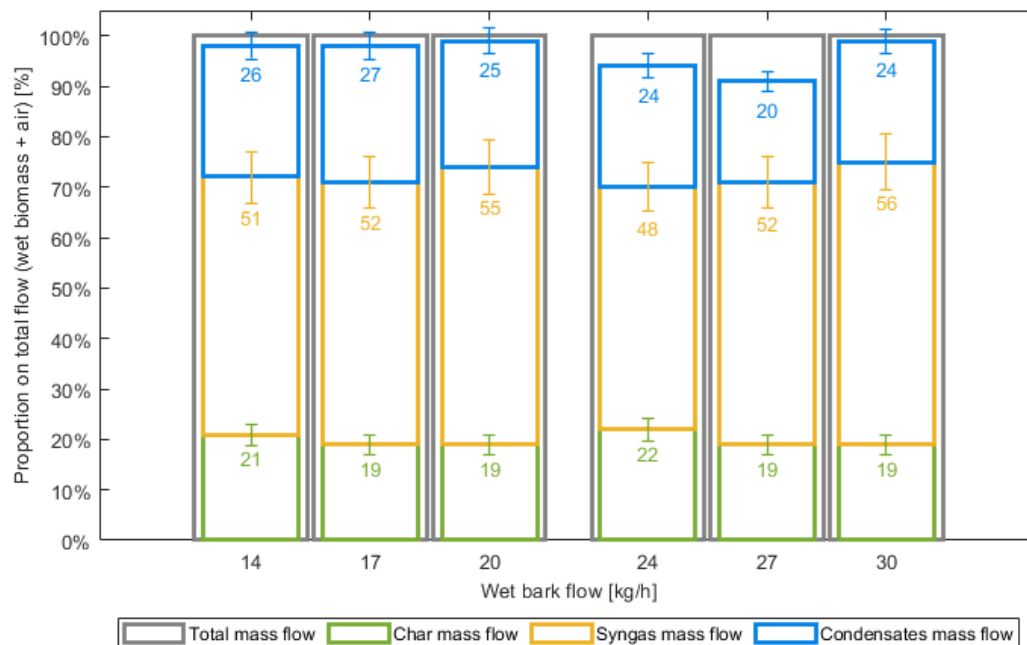


Fig. 9. Mass flow distribution

The difference between the total mass yield and the sum of the mass yields of biochar, condensate and syngas is due to an uncertainty in the mass measurement of these co-products. Thus, the difference in the temperature level reached by the bark between the minimum and maximum flow rates has moderate effect on the chemistry of biomass

conversion into pyrolysis co-products. The difference between the sum of char, syngas and condensates mass flow and the total mass flow represents the mass balance error.

This observation is confirmed by the yield of biochar on anhydrous shown in Fig. 10 which remains constant at about 38% regardless of the bark flow rate.

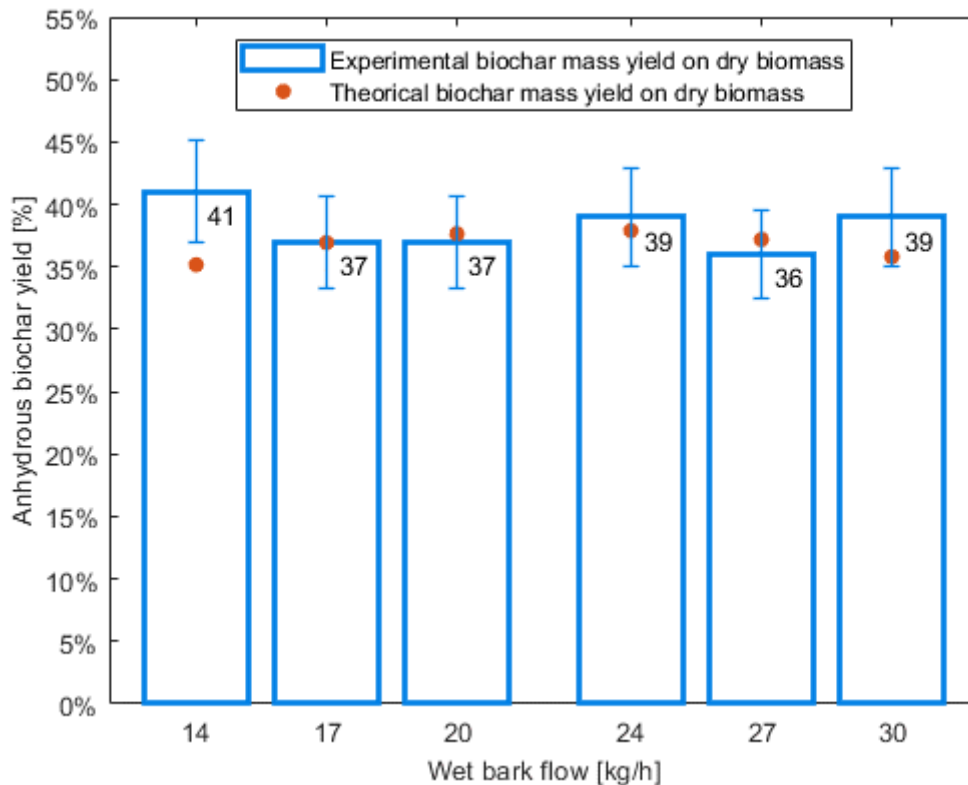


Fig. 10. Anhydrous biochar yield

3.4 Energy yields

The energy balance of the pyrolysis in process Fig. 11 is defined according to two co-products, syngas and biochar. The other heat flux correspond to the cooling of the gas, the various heat losses, the heating of the incoming air from ambient temperature to flame temperature and the drying of the bark. Like the mass yields, the energy yields are not very dependent on the bark flow. The difference in temperature level between the bark flows is therefore small enough not to significantly modify the thermochemical kinetics of pyrolysis. The differences

observed in the other heat fluxes are due to the varying ambient thermal conditions in the different tests. Some trials were indeed conducted in summer under favourable thermal conditions, while others were conducted in winter with colder and more humid ambient air.

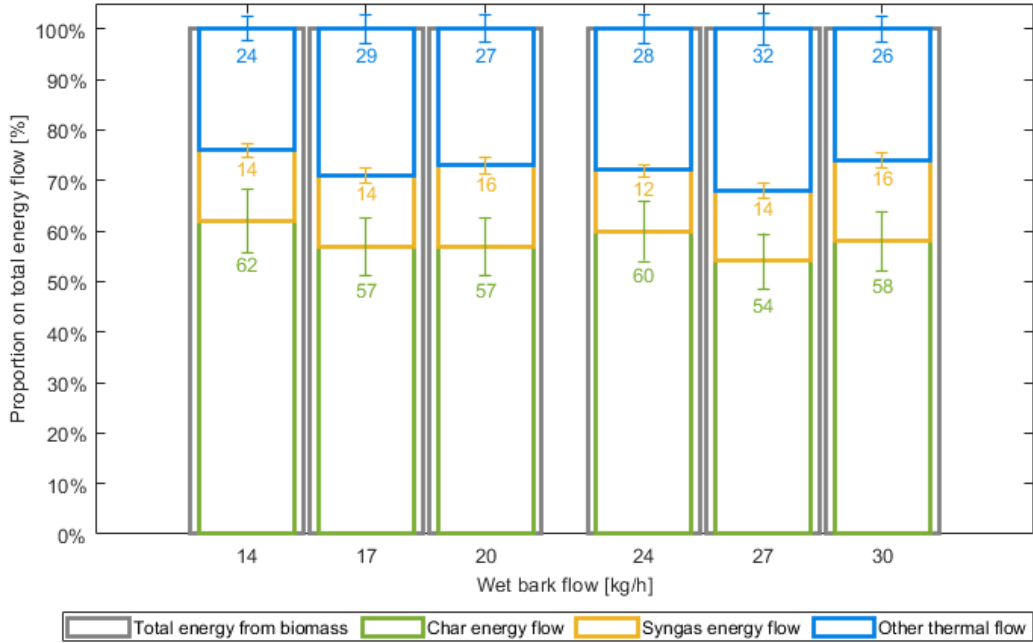


Fig. 11. Energy balance flow

3.5 Syngas composition

The composition of syngas in relation to mass and energy yields is neither very dependent on the flow rate over the range of bark flow rates considered. The average volumetric composition of syngas is 11% carbon monoxide, 19% carbon dioxide, 5% CH₄, 7% dihydrogen and 58% nitrogen. Each gas composition varies by less than 2% as a function of bark flow. The composition of the pyrolysis gas is therefore also not very dependent on the bark flow rate.

3.6 Equivalence ratio

The equivalence ratio referred by Ibrahim [28] or Panigrahy et al. [29] allows the characterisation of the pyrolyser as a whole (ie including partial combustion device) and the comparison of systems with total or partial combustion. Pyrolysis has an optimum equivalence ratio less than 0.2, gasification an equivalence ratio between 0.2 and 0.4 and combustion an equivalence ratio greater than 0.4 to 1.

The present prototype has a global equivalence ratio close to 0.1 as shown in Fig. 12. This ratio is compliant for a pyrolyser. This low equivalence ratio is due to the restriction of the air flow injected into the reactor due to its geometrical design. Indeed, increasing too much air in the furnace, the speed of the flow of air, pyrolysis gas and finally of syngas is such that the flame is blown downwards in the reactor, which can cause thermomechanical damage in the pipes allowing the evacuation of syngas. This phenomenon remains true over the range of bark flows tested.

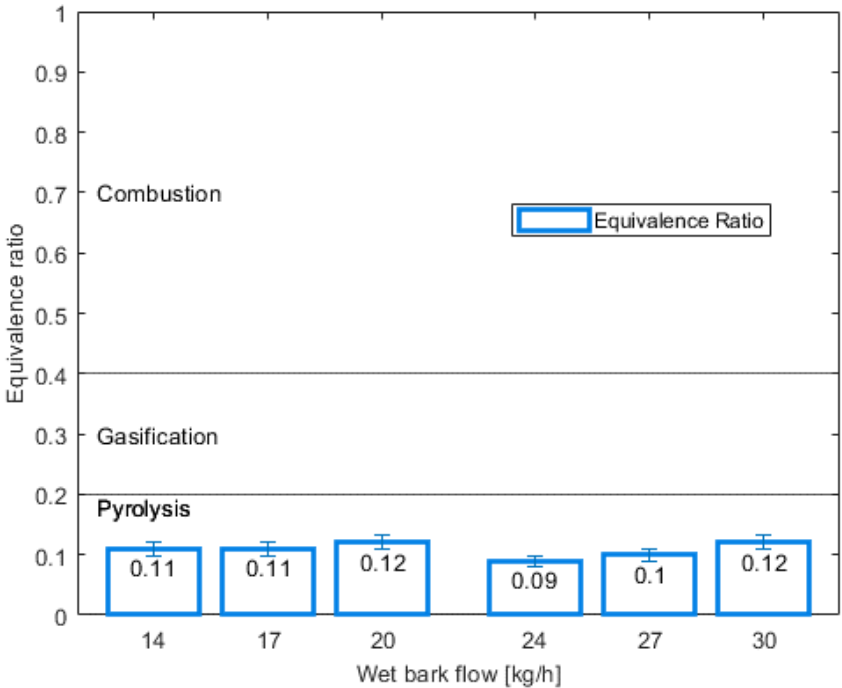


Fig. 12. Equivalence ratio

3.7 Biochar characteristics

The quality of biochar can be defined according to a multitude of parameters including fixed carbon content and specific surface area. The fixed carbon rate goes from 50% on a dry basis for biomass to 90% on a dry basis for biochar. Pyrolysis consumes little carbon, which is an advantage from the point of view of agronomic valorisation. The second interesting parameter is the development of the porosity corresponding to the specific surface. In the literature, Bouchelta et al. [30], Chekem, Lui et al. [31], Wang et al. [32] or Januszewicz et al. [33], show that each biomass has an optimum for each parameter (residence time, heating rate, pyrolysis temperature) allowing the best possible specific surface to be obtained. Below this optimum, not all volatiles are vaporised and above this optimum, the residence time and/or heating rate are too high and degrade the carbon structure. This optimum is also observed for bark pyrolysis with an optimum obtained for a wet bark flow of $20 \text{ kg} \cdot \text{h}^{-1}$ with a specific surface of $200 \text{ m}^2 \cdot \text{g}^{-1}$ as it shown in Fig. 11.

This optimum operating point is achieved at a heating rate of $19 \text{ K} \cdot \text{min}^{-1}$ and a residence time of $1\text{h}30$. A carbon content around 90% is observed on biochar samples from each test.

The objectives of the experimental study is to obtain a biochar with a specific surface as high as possible. This biochar, produced by pyrolysis alone as shown in Fig. 13, is however a good basis for producing a coal with a higher specific surface. Although the aim is not to produce an activated carbon, several authors have proposed chemical or thermal methods to increase

porosity. By choosing the most appropriate method, the biochar produced could go over $200 \text{ m}^2 \cdot \text{g}^{-1}$.

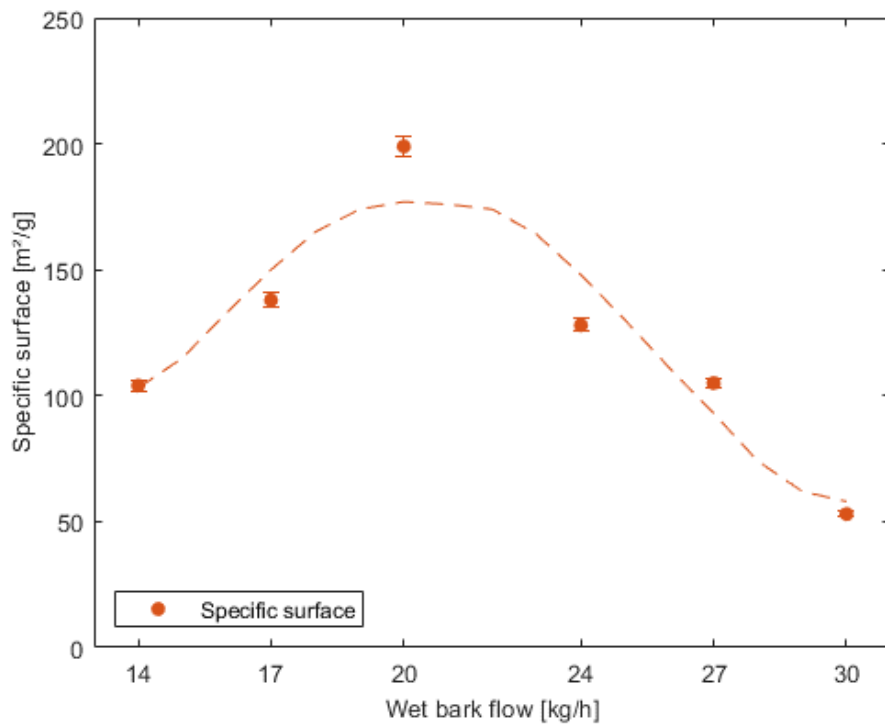


Fig. 13. Biochar specific surface

The quality of activation depends, as for pyrolysis, on the residence time or activation time put forward by Bouchelta et al. [30], temperature and heating rate, discussed by Bergna et al. [34]. There are several types of activation. Physical activation under oxidising agent flow (CO_2 , H_2O or both or O_2), chemical activation H_3PO_4 or KOH as Gueye [35] done in his work or by recovery of pyrolysis gases, the method of which is presented on the analysis of Langlois [36]. This solution is easily applicable to the prototype.

4 Conclusions and perspectives

The objectives of this study were to test a prototype pyrolysis process using bark to produce biochar and to build a numerical pyrolysis model to characterise the heat transfer and thermochemical conversion of biomass in a 6-material scheme (water, steam, wood, coke, gas and tar). Over the range of barks tested, the thermokinetic conditions of pyrolysis are sufficiently that no trends are observed in the evolution of gas and char yields and carbon content. The differences are however important in the development of porosity with specific surfaces varying from simple to quadruple and an optimum obtained for a flow rate of $20 \text{ kg} \cdot \text{h}^{-1}$.

In order to build the numerical model, the heat transfer by conduction and radiation was defined according to the effective thermal conductivity (ETC). A thermogravimetric analysis on bark powder was carried out by reproducing the experimental thermokinetic conditions of the prototype. This analysis allows to obtain pyrolysis kinetics and the parameters of the Arrhenius formalism. The experimental results, supplemented by a material characterisation phase, enabled the model to be matched with the experimental observations within an acceptable range (temperatures, mass yields, biomass mass loss, etc.).

In the prototype, a self-activation step by recovery of the pyrolysis gases will now be added after the pyrolysis zone in order to increase the development of the biochar porosity.

References

1. Werner C, Schmidt HP, Gerten D, Lucht W, Kammann C. Biogeochemical potential of biomass pyrolysis systems for limiting global warming to 1.5 °C. *Environ Res Lett.* 2018;
2. Shafizadeh F, Chin P. Thermal Deterioration of Wood. In: *Chemical Aspects, ACS Symp Ser.* 1977. p. 57-81.
3. Graham RG, Bergougnou MA, Freel BA. The kinetics of vapour-phase cellulose fast pyrolysis reactions. *Biomass Bioenergy.* 1994;7(1):33-47.
4. Richter F, Rein G. Pyrolysis kinetics and multi-objective inverse modelling of cellulose at the microscale. *Fire Saf J.* 2017;91:191-9.
5. Hameed S, Sharma A, Pareek V. A distributed activation energy model for cellulose pyrolysis in a fluidized bed reactor. *Chem Eng Res Des.* 2023;191:414-25.
6. Thurner F, Mann U. Kinetic Investigation of Wood Pyrolysis. *Ind Eng Chem Process Dev.* 1981;20.
7. Di Blasi C. Modeling and simulation of combustion processes of charring and non-charring solid fuels. *Prog Energy Combust Sci.* 1993;19(1):71-104.
8. Bryden KM, Ragland KW, Rutland CJ. Modeling thermally thick pyrolysis of wood. *Biomass Bioenergy.* 2002;22(1):41-53.
9. Lamarche P, Tazerout M, Gelix F, Köhler S, Mati K, Paviet F. Modelling of an indirectly heated fixed bed pyrolysis reactor of wood: Transition from batch to continuous staged gasification. *Fuel.* 2013;106:118-28.
10. Pinto O, Romero R, Carrier M, Appelt J, Segura C. Fast pyrolysis of tannins from pine bark as a renewable source of catechols. *J Anal Appl Pyrolysis.* 2018;136:69-76.
11. Jahiding M, Arsyad WOS, Rif'ah SM, Rizki RS, Mashuni. Effect of pyrolysis temperature on bio-fuel quality produced from pine bark (*Pinus merkusii*) by pyro-catalytics method. *J Phys Conf Ser.* 2021;1825(1):012047.
12. Wagenaar BM, Prins W, van Swaaij WPM. Flash pyrolysis kinetics of pine wood. *Fuel Process Technol.* 1993;36(1):291-8.
13. Blasi C, Branca C. Kinetics of Primary Product Formation from Wood Pyrolysis. *Ind Eng Chem Res - IND ENG CHEM RES.* 2001;40.
14. Tobo Y, Lotfi A, Virla LD, Mahinpey N. Fast pyrolysis multiphase CFD-kinetics model in a drop tube reactor. *Fuel.* 2023;340:127524.
15. Zhong Y, Ding Y, Lu K, Mao S, Li C. Kinetic parameters and reaction mechanism study of biomass pyrolysis by combined kinetics coupled with a heuristic optimization algorithm. *Fuel.* 2023;334:126622.

16. Ricoul F, Subrenat A, JOUBERT O, Le Gal La Salle A. Electricity production from lignocellulosic biomass by direct coupling of a gasifier and a nickel/yttria-stabilized zirconia-based solid oxide fuel cell: influence of the H₂S content of the syngas onto performances and aging. *J Solid State Electrochem.* 2018;22:1-12.
17. Daouk E. Etudes experimentale et numerique de la pyrolyse oxydante de la biomasse en lit fixe [PhD Thesis]. Ecole des Mines de Nantes Genie des procedes. Energetique et transferts; 2015.
18. Ragland KW, Aerts DJ, Baker AJ. Properties of wood for combustion analysis. *Bioresour Technol.* 1991;37(2):161-8.
19. TenWolde A, McNatt JD, Krahn L. Thermal properties of wood and wood panel products for use in buildings. Forest Service, Madison, WI (USA). Forest Products Lab.; 1988. Report No.: DOE/OR/21697-1.
20. Gupta M, Yang J, Roy C. Specific heat and thermal conductivity of softwood bark and softwood char particles. *Fuel.* 2003;82(8):919-27.
21. Perry RH, Green DW, Maloney JO. *Perry's Chemical engineers' handbook.* New York: McGraw-Hill; 1984.
22. Koufopoulos CA, Papayannakos N, Maschio G, Lucchesi A. Modelling of the pyrolysis of biomass particles. Studies on kinetics, thermal and heat transfer effects. *Can J Chem Eng.* 1991;69(4):907-15.
23. Kantorovich II, Bar-Ziv E. Heat transfer within highly porous chars: a review. *Fuel.* 1999;78(3):279-99.
24. Stamm AJ, Harris EE. *Chemical processing of wood,*. New York: Chemical Pub. Co.; 1953.
25. Tinney ER. The combustion of wooden dowels in heated air. *Symp Int Combust.* 1965;10(1):925-30.
26. Agarwal RK. On the use of the arrhenius equation to describe cellulose and wood pyrolysis. *Thermochim Acta.* 1985;91:343-9.
27. Roberts AF. The heat of reaction during the pyrolysis of wood. *Combust Flame.* 1971;17(1):79-86.
28. Ibrahim HAH. *Recent Advances in Pyrolysis.* BoD – Books on Demand; 2020. 124 p.
29. Panigrahy S, Liang J, Nagaraja SS, Zuo Z, Kim G, Dong S, et al. A comprehensive experimental and improved kinetic modeling study on the pyrolysis and oxidation of propyne. *Proc Combust Inst.* 2021;38(1):479-88.
30. Bouchelta C, Medjram MS, Zoubida M, Chekkat FA, Ramdane N, Bellat JP. Effects of pyrolysis conditions on the porous structure development of date pits activated carbon. *J Anal Appl Pyrolysis.* 2012;94:215-22.
31. Liu D, Jia B, Li S, Dong L, Gao J, Qin Y. Effect of pyrolysis conditions on the improvement of the physicochemical structure of activated carbon obtained from Jixi bituminous coal. *Asia-Pac J Chem Eng.* 2019;14.

32. Wang J, Wu FA, Wang M, Qiu N, Liang Y, Fang SQ, et al. Preparation of activated carbon from a renewable agricultural residue of pruning mulberry shoot. *Afr J Biotechnol.* 2010;9.
33. Januszewicz K, Kazimierski P, Klein M, Kardaś D, Łuczak J. Activated Carbon Produced by Pyrolysis of Waste Wood and Straw for Potential Wastewater Adsorption. *Materials.* 2020;13:2047.
34. Bergna D, Hu T, Prokkola H, Romar H, Lassi U. Effect of Some Process Parameters on the Main Properties of Activated Carbon Produced from Peat in a Lab-Scale Process. *Waste Biomass Valorization.* 2020;12.
35. Gueye M. Développement de charbon actif à partir de biomasses lignocellulosiques pour des applications dans le traitement de l'eau [PhD Thesis]. CIRAD; 2015.
36. Langlois S. Production de charbon activé par recouvrement des gaz de pyrolyse [PhD Thesis]. Université du Québec à Trois-Rivières; 2019.

5 Annex A

